

Article

Screening of II-IV-V₂ Materials for Photovoltaic Applications Based on Density Functional Theory Calculations

Byeong-Hyeon Jeong [†], Minwoo Jeong [†], Youbin Song , Kanghyeon Park  and Ji-Sang Park ^{*}

Department of Physics, Kyungpook National University, Daegu 41566, Korea; qudgus1431@knu.ac.kr (B.-H.J.); style4480@knu.ac.kr (M.J.); songyoubin@knu.ac.kr (Y.S.); kang-hyeon@knu.ac.kr (K.P.)

* Correspondence: jsparkphys@knu.ac.kr

† These authors contributed equally to this work.

Abstract: The relative stability of polymorphs and their electronic structure was investigated for II-IV-V₂ materials by using first-principles density functional theory calculations. Our calculation results show that, for Zn-, Cd-, and Be-containing compounds, nitrides favor the 2H polymorph with AB stacking sequence; however, phosphides, arsenides, and antimonides are more stable in the 3C polymorph with the ABC stacking sequence. The electronic band gap of materials was calculated by using hybrid density functional theory methods, and then materials with an ideal band gap for photovoltaic applications were chosen. The experimental synthesis of the screened materials is reported, except for CdSiSb₂, which was found to be unstable in our calculation. The absorption coefficient of the screened materials, especially ZnGeAs₂, was high enough to make thin-film solar cells. The higher stacking fault energy in ZnGeAs₂ than the others is consistent with the larger formation energy difference between the 2H and 3C polymorphs.

Keywords: semiconductor; solar cell; density functional theory



Citation: Jeong, B.-H.; Jeong, M.; Song, Y.; Park, K.; Park, J.-S. Screening of II-IV-V₂ Materials for Photovoltaic Applications Based on Density Functional Theory Calculations. *Crystals* **2021**, *11*, 883. <https://doi.org/10.3390/cryst11080883>

Academic Editor: Andreas Hermann

Received: 28 June 2021
Accepted: 27 July 2021
Published: 29 July 2021

Publisher's Note: MDPI stays neutral with regard to jurisdictional claims in published maps and institutional affiliations.



Copyright: © 2021 by the authors. Licensee MDPI, Basel, Switzerland. This article is an open access article distributed under the terms and conditions of the Creative Commons Attribution (CC BY) license (<https://creativecommons.org/licenses/by/4.0/>).

1. Introduction

The progress of photovoltaic technology has been largely due to the finding and optimization of new materials [1–4]. Among many approaches, cation mutation has remained a notable design principle for finding new materials [5]. Starting from diamond Si, we obtain zinc-blende CdTe (GaAs) that satisfies the octet rule by replacing every two Si atoms with Cd and Te (Ga and As). If two Cd atoms are replaced with Cu and In while Se substitutes for Te, then chalcopyrite CuInSe₂ is obtained as illustrated in Figure 1. If we further apply the operation, we can obtain kesterite Cu₂ZnSnSe₄. All of these materials were investigated extensively for photovoltaic applications both theoretically and experimentally [4]. II-IV-V₂ is another category of materials obtained by applying the design principle to III-V, while ZnSnN₂ is the most well-known material for photovoltaic application in this category [6].

Following the cation mutation principle, at least several tens of material can be made, theoretically, as many atoms have the same oxidation number. Such materials can be examined and screened by first-principles calculation as in previous studies [7–10]. There are many physical properties of constituent materials that determine the solar conversion efficiency [11–14]. Among them, the band gap is used as the most important metric to screen materials, as the solar conversion efficiency is fundamentally determined by the band gap [4,15].

Shaposhnikov et al. performed a comprehensive computational study of A^{II}B^{IV}C^V₂ semiconductors [16], and concluded that ZnSiAs₂ and ZnSnAs₂ are ideal for photovoltaic applications in terms of the high absorption coefficient and the dipole matrix, not the electronic band gap. To combinatorially generate the materials, Be, Mg, Zn, Cd, Si, Ge, Sn, P, and As were used but antimonides were not considered. More recently, Pandey et al. investigated other II-IV-V₂ materials computationally and suggested several candidates for photovoltaic applications [17]. In their study, the heat of the formation of materials

was calculated, using mBEEF meta-GGA functional [18], and then the electronic band gap was evaluated, using a semilocal GLLB-SC functional [19]. However, a specific exchange–correlation functional does not perfectly predict the ground structure of all materials, and therefore it is needed to double-check the prediction using other functionals [20–22]. Furthermore, Be was not included in the later study, even though Be also predominantly favors a 2+ oxidation state. It is also worth noting that BeO is stable in the wurtzite phase (2H), while BeS, BeSe, and BeTe are stable in the zinc-blende structure (3C) [23].

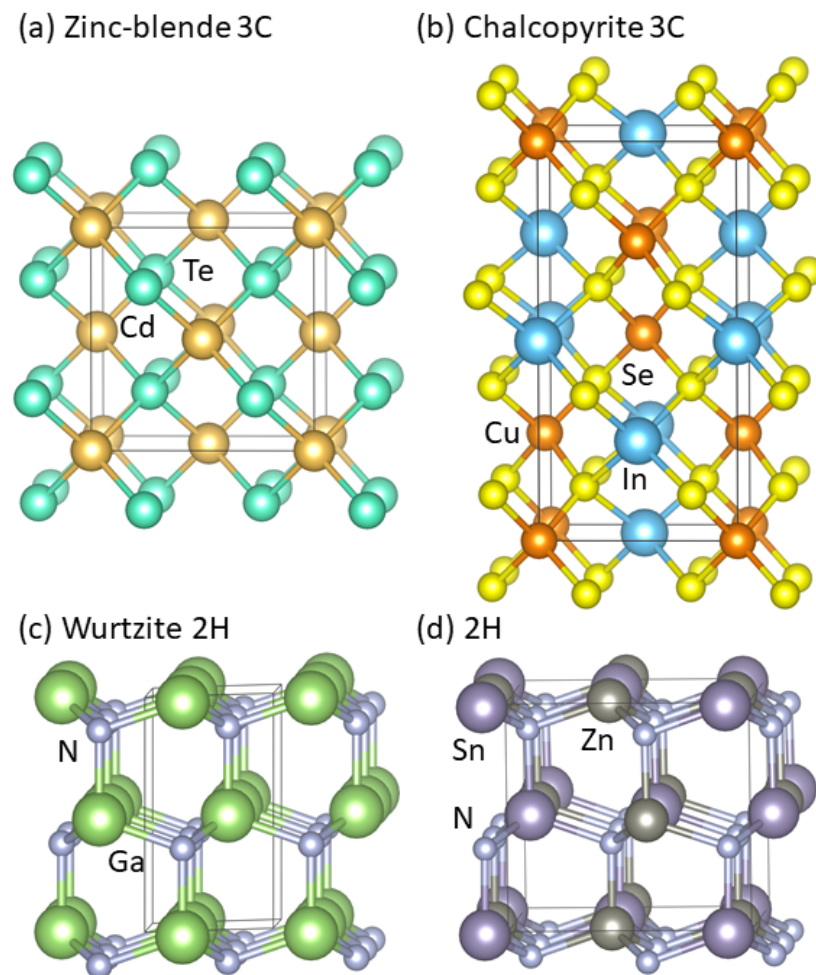


Figure 1. Atomic structure of (a) zinc-blende CdTe, (b) chalcopyrite CuInSe₂, (c) wurtzite GaN, and (d) ZnSnN₂. (Color online.)

In this article, we revisit the stability and the electronic structure of II-IV-V₂ materials to screen materials for photovoltaic applications. The relative formation energy of the 2H and the 3C polymorphs was determined by using three exchange–correlation functionals based on the majority voting. The electronic structure of the materials was calculated using a more stable structure at the hybrid density functional theory. The materials were selected based on the band gap, and the absorption coefficient of the screened materials was obtained accordingly. We also obtained the stacking fault energy for some screened materials for photovoltaic applications because the planar defects have critical roles in terms of transport properties [24,25].

2. Calculation Method

We performed first-principles DFT calculations using the projector-augmented wave (PAW) method [26], and implemented in the Vienna ab initio simulation package (VASP) [27]. We used three exchange–correlation functionals, such as LDA [28], SCAN+rVV10 [29], and

TPSS [30], to double-check the relative stability between polymorphs. The energy cutoff for the plane waves was set to 500 eV. A $6 \times 6 \times 6$ k -point grid was used for the primitive cells. The volume and the internal coordinates of atoms were fully relaxed until the residual forces were below 0.01 eV/Å. The electronic structure was investigated by using a hybrid density functional suggested by Heyd, Scuseria, and Ernzerhof (HSE06) [31]. For the HSE06 calculation, the energy cutoff was determined by setting the PREC tag to normal. A body-centered tetragonal unit cell of the 3C polymorph and an orthorhombic unit cell of the 2H polymorph were used throughout the study. The body-centered tetragonal and the orthorhombic cell unit cell contain 2 and 4 formula units, respectively.

3. Results and Discussion

ZnSnN₂ satisfies the octet rule because Zn, Sn, and N have +2, +4, −3 oxidation states, respectively. If each atom is replaced with an atom with the same oxidation state, the resulting material satisfies the octet rule as well. For instance, Zn can be replaced with Be or Cd, keeping the octet rule. Mg is another element that prefers +2 oxidation states, but we did not consider it because we restricted our focus to materials that are stable in the 2H and 3C polymorphs. MgO, MgS, and MgSe favor the rock-salt structure [23], and there is a report of a rock-salt type synthesis of MgSnN₂ [32]. Similarly, Si and Ge can substitute for Sn, while N sites can be occupied by P, As, and Sb atoms. The number of combinations satisfying the octet rule is 36.

This category of materials that consist of the tetrahedron is mostly stable in either of the 2H and the 3C polymorphs. To obtain which stacking sequence the materials favor, we compared the relative formation energy of II-IV-V₂ materials in the 2H and the 3C polymorphs. The relative formation energy of the 2H with respect to the 3C was calculated by using three different exchange-correlation functionals, as summarized in Figure 2.

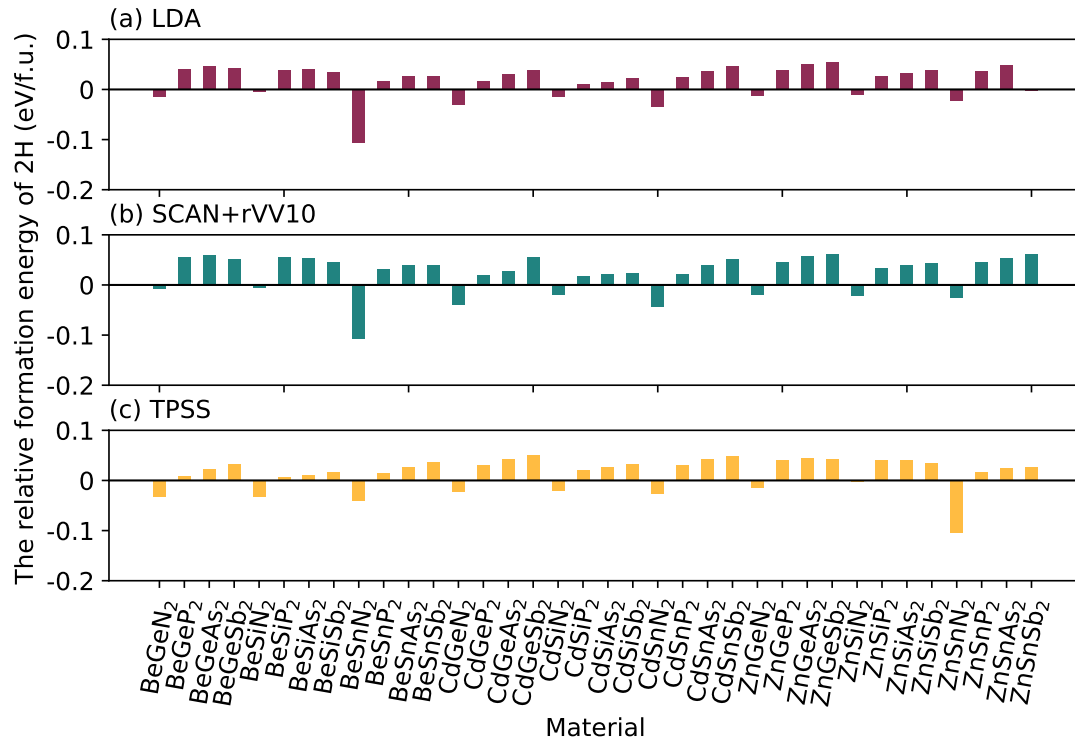


Figure 2. (a–c) The relative formation energy of material calculated by using LDA, SCAN+rVV10, and TPSS. The positive value means that the 3C polymorph has lower formation energy than the 2H polymorph.

Remarkably, every functional predicts that the same structure has lower formation energy. The only exception is ZnSnSb₂, which favored the 2H polymorph a little bit in our LDA calculation. However, in the other two calculations, the ZnSnSb₂ in the 3C polymorph

has lower energy than that in the 2H polymorph. Following the majority voting rule, we concluded that ZnSnSb_2 more favors the 3C structure than the 2H structure. Every nitride was calculated to be stable in the 2H polymorph; the phosphides, arsenides, and antimonides favored the 3C polymorph.

We performed hybrid DFT calculations in the 2H structure for nitride and the 3C for the others to obtain the electronic band gap, as summarized in Figure 3. We employed structures optimized by using SCAN+rVV10 functional for self-consistent field hybrid calculation. The optimized lattice constants were in good agreement with experimental values as summarized in Table 1. Some of the general chemical trends are as follows: If Zn is replaced with Cd, the band gap decreases on average, but on the other hand, the substitution of Be increases the band gap. The electronic band gap increases as Sn atoms are substituted with Ge and Si. The smaller the anion (Sb \rightarrow As \rightarrow P \rightarrow N), the larger the band gap obtained.

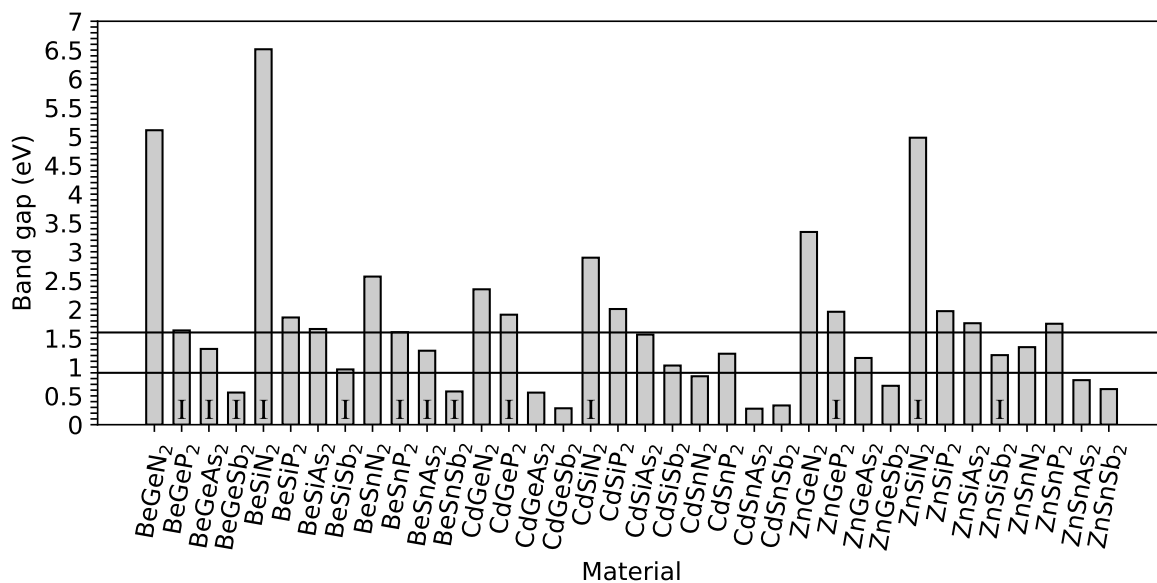


Figure 3. The calculated electronic band gap. Indirect band gap materials are denoted by I. (Color online.)

The ideal materials for photovoltaic applications should have a direct band gap between 1 eV and 1.5 eV [15]. We chose materials with a direct band gap between 0.9 eV and 1.6 eV, considering a potential error in the calculation. The following five materials satisfied the criteria: CdSnP_2 , ZnSnN_2 , ZnGeAs_2 , CdSiAs_2 , and CdSiSb_2 . The experimental synthesis of CdSiAs_2 , CdSnP_2 , ZnSnN_2 , and ZnGeAs_2 were reported in the literature [33–40]. Here, we note that CdSiAs_2 , CdSnP_2 , and ZnGeAs_2 received less attention, compared to ZnSnN_2 . Here, we also note that Pandey et al. suggested ZnSiSb_2 , ZnSnN_2 , and ZnSnP_2 as small band gap materials for tandem applications. However, in our calculation, ZnSiSb_2 has an indirect band gap and ZnSnP_2 has a band gap of about 1.75 eV, and is probably suitable for a larger band gap material in photovoltaic applications. As shown in Table 1, the calculated band gaps are in good agreement with the experimental studies.

On the other hand, we could not find any experimental study of CdSiSb_2 . To check whether CdSiSb_2 can be formed in the chalcopyrite structure, we obtained the heat of formation as follows:

$$\Delta H_f = E_{tot}(\text{CdSiSb}_2) - \mu_{\text{Cd}} - \mu_{\text{Si}} - 2\mu_{\text{Sb}}. \quad (1)$$

The chemical potential of Cd, Si, and Sb was obtained from hexagonal close-packed Cd, diamond Si, and trigonal Sb, respectively. In our SCAN+rVV10 calculation, the heat of the formation was calculated to be positive ($\Delta H_f = 0.35$ eV/f.u.), indicating that this material is not chemically stable. We double-checked the stability by using the LDA exchange–

correlation functional [22]; the calculation result was not changed ($\Delta H_f = 0.35$ eV/f.u.). This explains why there has been no experimental report of this material.

We employed the electronic band gap to screen materials; however, the absorption coefficient might be a more direct physical quantity to design solar cells. To obtain the absorption coefficient (α), we obtained the frequency-dependent dielectric function by performing hybrid DFT calculations. To reduce the computational cost, we employed a sparser k -point grid for the Fock potential by setting the reduction factor of 2 [41]. A $10 \times 10 \times 10$ k -point grid was used for ZnSnN₂. For the other three materials, a $14 \times 14 \times 14$ grid was employed.

Figure 4 shows the absorption coefficients of the four selected materials. CdSnP₂, CdSiAs₂, and ZnGeAs₂ show comparable absorption coefficients to the ordered ZnSnN₂ at wavelengths longer than 600 nm, and for the shorter wavelengths, the absorption coefficient is even higher. Among the four selected materials, ZnGeAs₂ has the highest absorption coefficient. This explains the motivation behind previous research studies to make solar cells based on these materials. Here, we point out that this class of materials is relatively new, compared to other mature technologies [6]. Further optimization should be made to improve efficiency, as solar conversion efficiency is a complex function of many parameters [12,13]. Here, we also point out that ZnSnN₂ is usually disordered and that the material properties are largely different from the ordered one considered in this study [42–44].

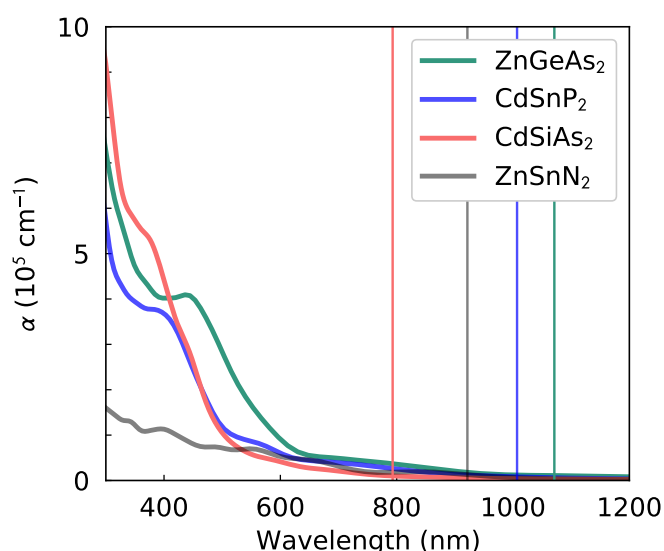


Figure 4. The calculated absorption coefficient of selected materials. The vertical lines represent the band gap energies. (Color online.)

The energy difference between the 2H and the 3C polymorphs is generally small as summarized in Figure 2. This small energy difference might cause the simultaneous formation of both polymorphs in the lattice. The stacking fault is a special case in that the metastable phase (the 2H or the 3C) is sandwiched in the host material. For instance, in the zinc-blende materials, the stacking fault can be regarded as a buried wurtzite phase. This planar defect can be formed in the host material by removing or inserting a layer (e.g., \cdots ABCABABC \cdots in the 3C). Both computational and experimental studies show that such planar defects are harmful in terms of carrier transport and defect accumulation [45–47].

To examine whether the stacking disorders likely happens in the selected materials, we obtained the stacking fault energy by using the SCAN+rVV10 exchange–correlation functional. We did not calculate the defect in ZnSnN₂ because we already investigated it in our previous study. According to our recent study, the stacking fault formation energy in ZnSnN₂ is about 0.28 eV/nm² [48]. In CdSnP₂, CdSiAs₂, and ZnGeAs₂, the stacking fault energy was 0.06 eV/nm², 0.15 eV/nm², and 0.47 eV/nm², respectively. The higher stacking fault energy in ZnGeAs₂ is well explained by the higher relative formation energy

of the 2H polymorph than the other two materials, as shown in Figure 2. The stacking fault can be formed in CdSnP₂ and CdSiAs₂ significantly, but much less formation is expected in ZnGeAs₂.

Table 1. Physical properties of the screened materials for single-junction solar cells. The lattice constants *a*, *b*, and *c* are those of the structure optimized by using SCAN+rVV10. The values in parentheses are experimental values. *E_g* and *E_{SFE}* stand for the electronic band gap and the stacking fault energy, respectively. The electronic band gap of ZnSnN₂ varies depending on the cation ordering [6].

Material	a (Å)	b (Å)	c (Å)	<i>E_g</i> (eV)	<i>E_{SFE}</i> (eV/nm ²)	Ref.
CdSnP ₂	5.896 (5.9015)	5.896 (5.9015)	11.548 (11.5144)	1.23 (1.165)	0.06	[33,49]
CdSiAs ₂	5.878 (5.8848)	5.878 (5.8848)	10.896 (10.8820)	1.56 (1.55)	0.15	[34,50]
ZnGeAs ₂	5.634 (5.672)	5.634 (5.672)	11.133 (11.153)	1.16 (1.15)	0.47	[51,52]
ZnSnN ₂	6.699 (6.8852)	5.822 (5.9557)	5.464 (5.5778)	1.35	0.28	[48] [53]

4. Summary

We revisited II-IV-V₂ materials for photovoltaic applications based on DFT calculations. Nitrides favor AB stacking sequence, but phosphides, arsenides, and antimonides prefer ABC stacking sequence. Five materials were calculated to have an ideal band gap for a single-junction solar cell, but CdSiSb₂ was not thermodynamically stable. The absorption coefficient of CdSnP₂, ZnSnN₂, ZnGeAs₂, and CdSiAs₂ was high enough to make thin-film solar cells. The stacking fault energy was low enough to be formed in CdSnP₂ and CdSiAs₂, but much higher in ZnGeAs₂.

Author Contributions: Conceptualization, J.-S.P.; Data curation, B.-H.J., M.J., Y.S. and K.P.; Formal analysis, B.-H.J., M.J., Y.S. and K.P.; Project administration, J.-S.P.; Supervision, J.-S.P.; Writing—Original draft, J.-S.P.; Writing—Review & editing, B.-H.J., M.J., Y.S., K.P. and J.-S.P. All authors have read and agreed to the published version of the manuscript.

Funding: This work was supported by National Research Foundation of Korea (NRF) grants funded by the Korea government (MSIT) (Nos. 2019M3D1A2104108 and 2020R1F1A1053606).

Institutional Review Board Statement: Not applicable.

Informed Consent Statement: Not applicable.

Data Availability Statement: The data presented in this study are available on request from the corresponding author.

Acknowledgments: This work was supported by the National Supercomputing Center with super-computing resources, including technical support (KSC-2020-CRE-0002).

Conflicts of Interest: The authors declare no conflict of interest.

References

- Okada, Y.; Ekins-Daukes, N.; Kita, T.; Tamaki, R.; Yoshida, M.; Pusch, A.; Hess, O.; Phillips, C.; Farrell, D.; Yoshida, K.; et al. Intermediate band solar cells: Recent progress and future directions. *Appl. Phys. Rev.* **2015**, *2*, 021302. [CrossRef]
- Haverkort, J.E.; Garnett, E.C.; Bakkers, E.P. Fundamentals of the nanowire solar cell: Optimization of the open circuit voltage. *Appl. Phys. Rev.* **2018**, *5*, 031106. [CrossRef]
- Li, S.; Li, C.Z.; Shi, M.; Chen, H. New phase for organic solar cell research: Emergence of Y-series electron acceptors and their perspectives. *ACS Energy Lett.* **2020**, *5*, 1554–1567. [CrossRef]
- Nayak, P.K.; Mahesh, S.; Snaith, H.J.; Cahen, D. Photovoltaic solar cell technologies: Analysing the state of the art. *Nat. Rev. Mater.* **2019**, *4*, 269–285. [CrossRef]

5. Walsh, A.; Chen, S.; Wei, S.H.; Gong, X.G. Kesterite thin-film solar cells: Advances in materials modelling of $\text{Cu}_2\text{ZnSnS}_4$. *Adv. Energy Mater.* **2012**, *2*, 400–409. [[CrossRef](#)]
6. Khan, I.S.; Heinselman, K.N.; Zakutayev, A. Review of ZnSnN_2 semiconductor material. *J. Phys. Energy* **2020**, *2*, 032007. [[CrossRef](#)]
7. Emery, A.A.; Wolverton, C. High-throughput dft calculations of formation energy, stability and oxygen vacancy formation energy of ABO_3 perovskites. *Sci. Data* **2017**, *4*, 1–10. [[CrossRef](#)]
8. Jain, A.; Voznyy, O.; Sargent, E.H. High-throughput screening of lead-free perovskite-like materials for optoelectronic applications. *J. Phys. Chem. C* **2017**, *121*, 7183–7187. [[CrossRef](#)]
9. Huo, Z.; Wei, S.H.; Yin, W.J. High-throughput screening of chalcogenide single perovskites by first-principles calculations for photovoltaics. *J. Phys. D Appl. Phys.* **2018**, *51*, 474003. [[CrossRef](#)]
10. Oganov, A.R.; Pickard, C.J.; Zhu, Q.; Needs, R.J. Structure prediction drives materials discovery. *Nat. Rev. Mater.* **2019**, *4*, 331–348. [[CrossRef](#)]
11. Niki, S.; Contreras, M.; Repins, I.; Powalla, M.; Kushiya, K.; Ishizuka, S.; Matsubara, K. CIGS absorbers and processes. *Prog. Photovolt. Res. Appl.* **2010**, *18*, 453–466. [[CrossRef](#)]
12. Crovetto, A.; Hansen, O. What is the band alignment of $\text{Cu}_2\text{ZnSn}(\text{S}, \text{Se})_4$ solar cells? *Sol. Energy Mater. Sol. Cells* **2017**, *169*, 177–194. [[CrossRef](#)]
13. Kanevce, A.; Reese, M.O.; Barnes, T.; Jensen, S.; Metzger, W. The roles of carrier concentration and interface, bulk, and grain-boundary recombination for 25% efficient CdTe solar cells. *J. Appl. Phys.* **2017**, *121*, 214506. [[CrossRef](#)]
14. Kurtz, S.; Repins, I.; Metzger, W.K.; Verlinden, P.J.; Huang, S.; Bowden, S.; Tappan, I.; Emery, K.; Kazmerski, L.L.; Levi, D. Historical analysis of champion photovoltaic module efficiencies. *IEEE J. Photovolt.* **2018**, *8*, 363–372. [[CrossRef](#)]
15. Shockley, W.; Queisser, H.J. Detailed balance limit of efficiency of p-n junction solar cells. *J. Appl. Phys.* **1961**, *32*, 510–519. [[CrossRef](#)]
16. Shaposhnikov, V.; Krivosheeva, A.; Borisenko, V.; Lazzari, J.L.; d’Avitaya, F.A. Ab initio modeling of the structural, electronic, and optical properties of $\text{A}^{\text{II}}\text{B}^{\text{IV}}\text{C}_2^{\text{V}}$ semiconductors. *Phys. Rev. B* **2012**, *85*, 205201. [[CrossRef](#)]
17. Pandey, M.; Kuhar, K.; Jacobsen, K.W. II–IV– V_2 and III–III– V_2 Polytypes as Light Absorbers for Single Junction and Tandem Photovoltaic Devices. *J. Phys. Chem. C* **2017**, *121*, 17780–17786. [[CrossRef](#)]
18. Wellendorff, J.; Lundgaard, K.T.; Jacobsen, K.W.; Bligaard, T. mBEEF: An accurate semi-local Bayesian error estimation density functional. *J. Chem. Phys.* **2014**, *140*, 144107. [[CrossRef](#)]
19. Gritsenko, O.; van Leeuwen, R.; van Lenthe, E.; Baerends, E.J. Self-consistent approximation to the Kohn-Sham exchange potential. *Phys. Rev. A* **1995**, *51*, 1944. [[CrossRef](#)]
20. Zhang, Y.; Kitchaev, D.A.; Yang, J.; Chen, T.; Dacek, S.T.; Sarmiento-Pérez, R.A.; Marques, M.A.; Peng, H.; Ceder, G.; Perdew, J.P.; et al. Efficient first-principles prediction of solid stability: Towards chemical accuracy. *Npj Comput. Mater.* **2018**, *4*, 1–6. [[CrossRef](#)]
21. Yang, J.H.; Kitchaev, D.A.; Ceder, G. Rationalizing accurate structure prediction in the meta-GGA SCAN functional. *Phys. Rev. B* **2019**, *100*, 035132. [[CrossRef](#)]
22. Park, J.S. Comparison study of exchange-correlation functionals on prediction of ground states and structural properties. *Curr. Appl. Phys.* **2021**, *22*, 61–64. [[CrossRef](#)]
23. Wyckoff, R.W.G. *Crystal Structures*; Interscience Publishers: New York, NY, USA, 1965; Volume 1
24. Park, J.S.; Walsh, A. Modeling Grain Boundaries in Polycrystalline Halide Perovskite Solar Cells. *Annu. Rev. Condens. Matter Phys.* **2020**, *12*, 95–109. [[CrossRef](#)]
25. Park, J.S.; Li, Z.; Wilson, J.N.; Yin, W.J.; Walsh, A. Hexagonal Stacking Faults Act as Hole-Blocking Layers in Lead Halide Perovskites. *ACS Energy Lett.* **2020**, *5*, 2231–2233. [[CrossRef](#)]
26. Blöchl, P.E. Projector augmented-wave method. *Phys. Rev. B* **1994**, *50*, 17953. [[CrossRef](#)] [[PubMed](#)]
27. Kresse, G.; Furthmüller, J. Efficient iterative schemes for ab initio total-energy calculations using a plane-wave basis set. *Phys. Rev. B* **1996**, *54*, 11169. [[CrossRef](#)] [[PubMed](#)]
28. Ceperley, D.M.; Alder, B.J. Ground state of the electron gas by a stochastic method. *Phys. Rev. Lett.* **1980**, *45*, 566. [[CrossRef](#)]
29. Peng, H.; Yang, Z.H.; Perdew, J.P.; Sun, J. Versatile van der Waals density functional based on a meta-generalized gradient approximation. *Phys. Rev. X* **2016**, *6*, 041005. [[CrossRef](#)]
30. Tao, J.; Perdew, J.P.; Staroverov, V.N.; Scuseria, G.E. Climbing the density functional ladder: Nonempirical meta-generalized gradient approximation designed for molecules and solids. *Phys. Rev. Lett.* **2003**, *91*, 146401. [[CrossRef](#)]
31. Heyd, J.; Scuseria, G.E.; Ernzerhof, M. Hybrid functionals based on a screened Coulomb potential. *J. Chem. Phys.* **2003**, *118*, 8207–8215. [[CrossRef](#)]
32. Kawamura, F.; Imura, M.; Murata, H.; Yamada, N.; Taniguchi, T. Synthesis of a Novel Rocksalt-Type Ternary Nitride Semiconductor MgSnN_2 Using the Metathesis Reaction Under High Pressure. *Eur. J. Inorg. Chem.* **2020**, *2020*, 446–451. [[CrossRef](#)]
33. Reddy, N.; Kistaiah, P.; Murthy, K. High-temperature thermal expansion study of cadmium stannidiphosphide by an X-ray method. *J. Phys. D Appl. Phys.* **1982**, *15*, 2247. [[CrossRef](#)]
34. Avirović, M.; Lux-Steiner, M.; Elrod, U.; Hönigschmid, J.; Bucher, E. Single crystal growth of CdSiAs_2 by chemical vapor transport; its structure and electrical properties. *J. Cryst. Growth* **1984**, *67*, 185–194. [[CrossRef](#)]

35. Chelluri, B.; Chang, T.; Ourmazd, A.; Dayem, A.; Zyskind, J.; Srivastava, A. Molecular beam epitaxial growth of II–V semiconductor Zn_3As_2 and II–IV–V chalcopyrite ZnGeAs_2 . *J. Cryst. Growth* **1987**, *81*, 530–535. [[CrossRef](#)]
36. Kimmel, M.; Lux-Steiner, M.; Vögt, M.; Bucher, E. n-ZnO/p-CdSiAs₂ heterojunction solar cells. *J. Appl. Phys.* **1988**, *64*, 1560–1561. [[CrossRef](#)]
37. Feldberg, N.; Aldous, J.; Linhart, W.; Phillips, L.; Durose, K.; Stampe, P.; Kennedy, R.; Scanlon, D.; Vardar, G.; Field, R., III; et al. Growth, disorder, and physical properties of ZnSnN_2 . *Appl. Phys. Lett.* **2013**, *103*, 042109. [[CrossRef](#)]
38. Peshek, T.J.; Zhang, L.; Singh, R.K.; Tang, Z.; Vahidi, M.; To, B.; Coutts, T.J.; Gessert, T.A.; Newman, N.; Van Schilfgaarde, M. Criteria for improving the properties of ZnGeAs_2 solar cells. *Prog. Photovolt. Res. Appl.* **2013**, *21*, 906–917. [[CrossRef](#)]
39. Martinez, A.D.; Fioretti, A.N.; Toberer, E.S.; Tamboli, A.C. Synthesis, structure, and optoelectronic properties of II–IV–V₂ materials. *J. Mater. Chem. A* **2017**, *5*, 11418–11435. [[CrossRef](#)]
40. Nakatsuka, S.; Inoue, R.; Nose, Y. Fabrication of CdSnP_2 Thin Films by Phosphidation for Photovoltaic Application. *ACS Appl. Energy Mater.* **2018**, *1*, 1635–1640. [[CrossRef](#)]
41. Park, J.S. Examination of high-throughput hybrid calculations using coarser reciprocal space meshes. *Curr. Appl. Phys.* **2020**, *20*, 379–383. [[CrossRef](#)]
42. Veal, T.D.; Feldberg, N.; Quackenbush, N.F.; Linhart, W.M.; Scanlon, D.O.; Piper, L.F.; Durbin, S.M. Band gap dependence on cation disorder in ZnSnN_2 solar absorber. *Adv. Energy Mater.* **2015**, *5*, 1501462. [[CrossRef](#)]
43. Quayle, P.C.; Blanton, E.W.; Punya, A.; Junno, G.T.; He, K.; Han, L.; Zhao, H.; Shan, J.; Lambrecht, W.R.; Kash, K. Charge-neutral disorder and polytypes in heterovalent wurtzite-based ternary semiconductors: The importance of the octet rule. *Phys. Rev. B* **2015**, *91*, 205207. [[CrossRef](#)]
44. Lany, S.; Fioretti, A.N.; Zawadzki, P.P.; Schelhas, L.T.; Toberer, E.S.; Zakutayev, A.; Tamboli, A.C. Monte Carlo simulations of disorder in ZnSnN_2 and the effects on the electronic structure. *Phys. Rev. Mater.* **2017**, *1*, 035401. [[CrossRef](#)]
45. Sun, C.; Lu, N.; Wang, J.; Lee, J.; Peng, X.; Klie, R.F.; Kim, M.J. Creating a single twin boundary between two CdTe (111) wafers with controlled rotation angle by wafer bonding. *Appl. Phys. Lett.* **2013**, *103*, 252104. [[CrossRef](#)]
46. Park, J.S.; Kim, S.; Walsh, A. Opposing effects of stacking faults and antisite domain boundaries on the conduction band edge in kesterite quaternary semiconductors. *Phys. Rev. Mater.* **2018**, *2*, 014602. [[CrossRef](#)]
47. Li, W.; Rothmann, M.U.; Zhu, Y.; Chen, W.; Yang, C.; Yuan, Y.; Choo, Y.Y.; Wen, X.; Cheng, Y.B.; Bach, U.; et al. The critical role of composition-dependent intragrain planar defects in the performance of $\text{MA}_{1-x}\text{FA}_x\text{PbI}_3$ perovskite solar cells. *Nat. Energy* **2021**, *6*, 624–632. [[CrossRef](#)]
48. Jeong, B.H.; Park, J.S. Stability and electronic structure of stacking faults and polytypes in ZnSnN_2 , ZnGeN_2 , and ZnSiN_2 . *J. Korean Phys. Soc.* **2021**. [[CrossRef](#)]
49. Pikhtin, A.; Razbegaev, V.; Goryunova, N.; Leonov, E.; Orlov, V.; Karavaev, G.; Poplavnoi, A.; Chaldyshev, V. Energy band structure and optical properties of CdSnP_2 . *Phys. Status Solidi A* **1971**, *4*, 311–318. [[CrossRef](#)]
50. Shay, J.; Buehler, E. Electroreflectance Spectra of CdSiAs_2 and CdGeAs_2 . *Phys. Rev. B* **1971**, *3*, 2598. [[CrossRef](#)]
51. Shah, S.; Greene, J. Growth and physical properties of ZnGeAs_2 . *Mater. Lett.* **1983**, *2*, 115–118. [[CrossRef](#)]
52. Peshek, T.; Tang, Z.; Zhang, L.; Singh, R.; To, B.; Gessert, T.; Coutts, T.; Newman, N.; Van Schilfgaarde, M. ZnGeAs_2 thin films properties: A potentially useful semiconductor for photovoltaic applications. In Proceedings of the 2009 34th IEEE Photovoltaic Specialists Conference (PVSC), Philadelphia, PA, USA, 7–12 June 2009; pp. 001367–001369.
53. Senabulya, N.; Feldberg, N.; Makin, R.A.; Yang, Y.; Shi, G.; Jones, C.M.; Kioupakis, E.; Mathis, J.; Clarke, R.; Durbin, S.M. Stabilization of orthorhombic phase in single-crystal ZnSnN_2 films. *AIP Adv.* **2016**, *6*, 075019. [[CrossRef](#)]